

The signatures of the outer Lindblad resonance and corotation of a large Galactic bar in local velocity space

G. Monari¹, B. Famaey², A. Siebert², C. Wegg³, and O. Gerhard⁴

¹ Leibniz Institut fuer Astrophysik Potsdam (AIP), An der Sternwarte 16, 14482 Potsdam, Germany
e-mail: gmonari@aip.de

² Université de Strasbourg, CNRS UMR 7550, Observatoire astronomique de Strasbourg, 11 rue de l'Université, 67000 Strasbourg, France

³ Université Côte d'Azur, Observatoire de la Côte d'Azur, CNRS, Laboratoire Lagrange, Bd de l'Observatoire, CS 34229, 06304 Nice cedex 4, France

⁴ Max-Planck-Institut für extraterrestrische Physik, Gießenbachstraße 1, 85748 Garching bei München, Germany

Received xxxx; accepted xxxx

ABSTRACT

The second data release of the Gaia mission has revealed a very rich structure in local velocity space, which is related to resonances with multiple non-axisymmetric patterns and possibly to incomplete phase-mixing. In terms of in-plane motions, this rich structure is also seen as ridges in the actions of the axisymmetric background potential of the Galaxy. We have recently developed a method to capture the behaviour of the stellar phase-space distribution function at a resonance, by re-expressing it in terms of a new set of canonical actions and angles variables valid in the resonant region. At least some of the action space ridges seen in Gaia data must obviously be linked to resonances with the central bar of the Galaxy. However, the structure and pattern speed of the bar have been heavily debated in recent years. Here, by properly treating the distribution function at resonances, and by using a realistic model for the Galactic bar, we confirm that orbits trapped at the corotation of a slowly rotating large bar produce a structure akin to the Hercules moving group in local velocity space (Pérez-Villegas et al. 2017). We additionally show that a second prominent ridge in action space then corresponds to the 4:1 outer resonance of the $m = 4$ mode of such a bar, and that the velocity structure seen as an arch at high azimuthal velocities in Gaia data can be related to its 2:1 outer Lindblad resonance.

Key words. Galaxy: kinematics and dynamics – Galaxy: disc – Galaxy: solar neighborhood – Galaxy: structure – Galaxy: evolution

1. Introduction

The local velocity distribution of stars near the Sun has long been known to exhibit clear substructures most likely associated with resonances with multiple non-axisymmetric patterns (e.g. Dehnen 1998; Famaey et al. 2005) and possibly incomplete phase-mixing (Minchev et al. 2009). The second data release from the Gaia mission has now revealed this rich network of substructures with unprecedented details, displaying multiple clearly defined ridges in local velocity space (Gaia Collaboration et al. 2018), and even vertical velocity disturbances (Antoja et al. 2018; Monari et al. 2018), which could be associated to the perturbation of the disk by the Sagittarius dwarf galaxy (Laporte et al. 2018, e.g.) or the buckling of the Galactic bar (Khoperskov et al. 2018). As far as in-plane motions are concerned, it is also interesting to consider the distribution of stars in the space of actions, which are adiabatic invariant integrals of the motion constituting the natural coordinate system for Galactic dynamics and perturbation theory. Trick et al. (2018) produced such plots in various volumes around the Sun. For local stars ($d < 200$ pc), they revealed several prominent ridges in the radial action distribution, among which one at the lowest border of the local azimuthal action (angular momentum) distribution, corresponding to the well-known Hercules moving group at low azimuthal velocities, and one at high angular momentum, corresponding to an arch at high velocities “covering” the velocity ellipsoid from

above at $V \sim 40 \text{ km s}^{-1}$, where V is the heliocentric tangential velocity.

The Hercules moving group, in particular, has long been suspected to be associated to the perturbation of the potential by the central bar of the Galaxy (Dehnen 1999b, 2000). If the Sun is located just outside the bar’s outer Lindblad resonance (OLR), where stars make two epicyclic oscillations while making one retrograde rotation in the frame of the bar, the Hercules moving group is naturally generated by the linear deformation of the unperturbed background phase-space distribution function (DF). This however implies a rather fast pattern speed for the bar, of the order of $\Omega_b = 53 \text{ km s}^{-1} \text{ kpc}^{-1}$. By solving the linearized Boltzmann equation in the presence of the simple quadrupole bar potential of Dehnen (2000), we could show in Monari et al. (2016, 2017b,c) that the Hercules moving group was indeed naturally formed outside of the bar’s OLR, and that its observed position in velocity space was varying as predicted by such a model. However, both the three-dimensional density of red clump giants (Wegg et al. 2015) and the gas kinematics in the inner Galaxy (Sormani et al. 2015) indicate that the pattern speed of the Galactic bar could be, in fact, significantly slower. From dynamical modelling of the stellar kinematics in the inner Galaxy, (Portail et al. 2017, hereafter P17), deduced a pattern speed of $\Omega_b = 39 \text{ km s}^{-1} \text{ kpc}^{-1}$. Pérez-Villegas et al. (2017) then showed, with orbit simulations in the potential of P17, that stars trapped at the co-rotation resonance of such a bar could also reproduce the Hercules position in local velocity space.

In Monari et al. (2017a, hereafter M17), we developed an analytical method to capture the behaviour of the stellar phase-space DF at a resonance, where the linearisation of the collisionless Boltzmann equation yields a divergent solution (problem of small divisors). This is indeed a fundamental difference between a model in which the Sun is located outside of the bar’s OLR and one where it is outside of the bar’s corotation (CR) as in P17. Indeed, while the Hercules moving group is located outside of the trapping region in the former case, and can be treated through linearisation of the Boltzmann equation (Monari et al. 2016, 2017b,c), it is precisely located in the resonant trapping region for a slow bar like that of P17. However, with the M17 method, the deformation of velocity space induced by Dehnen’s bar potential with a slow pattern speed was found to be rather minor. Here, by using the actual bar potential of P17 instead, and by computing the distribution function in the CR and OLR regions, we confirm that the Hercules moving group can indeed be reproduced, and that the OLR also induces a prominent ridge in radial actions at high angular momentum, corresponding to the arch on top of the velocity ellipsoid observed in local velocity space with Gaia. Additionally, the 4:1 resonance generates a third ridge close to the center. At least three of the most prominent features in local action space can thus in principle be naturally reproduced solely by a slow bar model with $\Omega_b = 39 \text{ km s}^{-1} \text{ kpc}^{-1}$.

In Sect. 2, we present the Galactic potential of P17 and our extraction of its Fourier modes. We then summarize in Sect. 3 the M17 method to treat the behaviour of the DF at resonances, and we apply in Sect. 4 this method to the CR and OLR of the $m = 2$ mode, as well as to the 4:1 outer resonance of the $m = 4$ mode of the P17 potential. We then validate our analytical treatment with numerical orbit integrations in Sect. 5, and we conclude in Sect. 6.

2. The distribution function in resonant regions: action-angle formalism

Let (J_R, J_ϕ) be the radial and azimuthal actions and (θ_R, θ_ϕ) the canonically conjugated radial and azimuthal angles, defined in the background axisymmetric potential Φ_0 . A star’s actions and angles (from now on AA) are obtained as combinations of the star’s positions and velocities, and they are particularly convenient phase-space coordinates for several reasons, listed in Binney & Tremaine (2008). In particular, the equilibrium axisymmetric background DF can be written purely as a function of the actions from Jeans’ theorem, and they are the most convenient coordinates for perturbation theory. In simple words, the actions identify a star’s orbit in phase-space, whilst the angles denote the phase of the star on that particular orbit. The larger the radial action J_R is, the more energetic its radial excursions are, and the more eccentric the orbit is. The azimuthal action J_ϕ represents the vertical component of the angular momentum L_z . Here, we approximate the true values of the AA using the epicyclic approximation (Binney & Tremaine 2008, M17). In further work, we will extend the present modelling to more realistic AA variables obtained through a combination of the Torus Machinery (e.g. Binney & McMillan 2016) to go from AA variables to positions and velocities, and of the ‘Stäckel fudge’ (e.g. Binney 2012; Sanders & Binney 2016) for the reverse transformation. For this reason, the results obtained in this letter are still not fully quantitative, and we will confirm them in Sect. 5 with backward orbit integrations not making use of the AA variables in computing the response of the DF to the bar perturbation.

Using the AA and the Galactic frequencies Ω and κ , we can define an ‘unperturbed’ DF for the Galactic disc, i.e. a DF

that would not change in time, because of the Jeans theorem, if there was no bar perturbation, which we denote $f_0(J_R, J_\phi)$. As in M17, we choose the quasi-isothermal DF defined by Binney & McMillan (2011), with a scale length of 2 kpc, a velocity dispersion scale-length of 10 kpc, and a local velocity dispersion $\sigma_R(R_0) = 45 \text{ km s}^{-1}$ (slightly hotter than in M17).

The response of the unperturbed DF to the bar potential is strongest at the resonances, that happen at the locations of phase space where

$$l\omega_R(J_R, J_\phi) + m[\omega_\phi(J_R, J_\phi) - \Omega_b] = 0. \quad (1)$$

where $\omega_R = \dot{\theta}_R$ and $\omega_\phi = \dot{\theta}_\phi$ are the orbital frequencies, and simply become, in the epicyclic approximation, $\omega_R = \kappa(R_g)$ and $\omega_\phi = \Omega(R_g) + [\kappa(R_g)/J_\phi]J_R$, where $R_g(J_\phi)$ is the guiding radius (Dehnen 1999a). For simplicity we only consider the unperturbed part of the potential, $\Phi_0(R)$, and its $m = 2$ and $m = 4$ modes, which are the dominant ones in the bar potential.

In Eq. (1), we will consider the $(l, m) = (0, 2)$ resonance, namely the CR, and the $(l, m) = (1, 2)$, namely the OLR. We shall also treat the $(l, m) = (1, 4)$ resonance of the $m = 4$ Fourier mode of the potential.

To study the response of f_0 near a resonance, we have to go through a first canonical transformation of coordinates, from the old AA $(J_R, J_\phi, \theta_R, \theta_\phi)$ to new ‘fast’ and ‘slow’ AA $(J_f, J_s, \theta_f, \theta_s)$. The canonical transformation is (Weinberg 1994, M17):

$$\begin{aligned} \theta_s &= l\theta_R + m(\theta_\phi - \Omega_b t), & J_\phi &= mJ_s, \\ \theta_f &= \theta_R, & J_R &= lJ_s + J_f, \end{aligned} \quad (2)$$

where $(l, m) = [(0, 2), (1, 2), (1, 4)]$ for the CR, OLR, and 4:1 resonance respectively. The angle θ_s is called the ‘slow angle’ because it evolves slowly near a resonance, as is evident from the definition of the frequencies and that of the resonance in Eq. (1). On the other hand, θ_f changes more rapidly and is called the ‘fast angle’. Physically, the slow angle θ_s represents the azimuth of the apocentre of the orbit in the reference frame where the unperturbed orbit would be close to the resonance. Therefore, θ_s represents the angle of precession of the orbit. At this point, expanding the potential in AA coordinates, it is possible to show that, near the resonances, J_f is almost constant along a star’s orbit, and that one can average the Hamiltonian over the fast angles. For each value of J_f , the motion in θ_s then becomes approximately a pendulum one, with $J_s(t)$ the momentum of the pendulum. The steps to show this are explained in detail in M17. One can then define a pendulum energy parameter k depending on the phase-space coordinates, that determines whether the pendulum is ‘librating’ (i.e. the θ_s angle oscillates back and forth between a maximum and a minimum without ever covering the whole $[0, 2\pi]$ range), or ‘circulating’ (i.e. θ_s has a motion that covers the whole range of angles). Stars at a position of phase-space where the θ_s pendulum is librating are called ‘trapped to the resonances’.

For a pendulum, it is of course possible to make a new canonical transformation defining the actual AA of the pendulum itself: (θ_p, J_p) . The way these depend on the phase-space coordinates changes according to whether the orbit is trapped or not. The pendulum AA define also the motion in $J_s(\theta_p, J_p)$ nearby the resonances. We can therefore rewrite the unperturbed DF as $f_0(J_f, J_s(\theta_p, J_p))$.

In M17 (see also Binney 2018), the perturbed DF close to the resonances was then defined as the original DF phase-mixed over the angles θ_p

$$f = \langle f_0(J_f, J_s(\theta_p, J_p)) \rangle, \quad (3)$$

where the average is done over the angle θ_p . Outside the zone of resonance, the DF is instead described as

$$f = f_0(J_f, \langle J_s(\theta_p, J_p) \rangle), \quad (4)$$

where, in this case, the average represents the average J_s of the circulating motion. Note that these recipes to obtain the perturbed DF are, in principle, different for every resonance also outside of the regions of trapping, while we want here to describe simultaneously the CR, 2:1 OLR, and 4:1 resonance of the Galactic bar. However, the value obtained outside the zone of resonance for f is very similar in the case of the three resonances, because the J_s oscillations amplitudes decrease fast going away from the resonant zone. It is therefore sufficient to take, outside the resonant regions of the phase space, the mean of the three DFs obtained with the three resonances.

3. Results

As in M17, we will concentrate hereafter on computing the perturbed DF at a few configuration space points, scanning through velocity space in order to define, at each phase-space point, the pendulum equation of motion for θ_s and its associated AA coordinates (J_p, θ_p) . In considering a large volume around the Sun, the same procedure should be iterated on a very tight grid of configuration space points, and one should take into account a well-defined selection function. This will be the topic of further works.

Here, we start by plotting the perturbed DF as a function of the coordinates of velocity space, at three particular points of the configuration space, $R = R_0 = 8.2$ kpc, $R = 8.6$ kpc, and $R = 9$ kpc, all at the azimuth of the Sun. In Fig. 1 we plot the DF in (u, v) coordinates, namely the Galactocentric radial velocity in the direction of the Galactic center, and the peculiar tangential velocity with respect to the circular one.

As can clearly be seen on this figure, all three main resonances are present as deformations of the velocity distribution, that would be otherwise smooth. In particular the effect of the CR is to form an Hercules-like moving group (Pérez-Villegas et al. 2017) that is centred at $(u, v) \simeq (-25, -50)$ km s⁻¹ at $R = 8.2$ kpc and that shifts at lower v and becomes less populated as R increases, like the Hercules moving group does in the real data. At the same time, the OLR forms a structure similar to the arch present at high azimuthal velocities in Gaia data, which extends in the model between $(u, v) \simeq (-50, 50)$ km s⁻¹ and $(u, v) \simeq (50, 50)$ km s⁻¹. As in the case of the CR, and as expected, this structure shifts at lower v for increasing R . Finally, the 4:1 resonance deforms the velocity ellipsoid close to the center of the v distribution.

To show even more clearly these structures, in Fig. 2 we show the DF, at the same locations in configuration space as in Fig. 1, but this time in the (J_R, J_ϕ) action space of the unperturbed axisymmetric background. In this case, the deformation due to the CR appears clearly as the stripe for $J_\phi - J_{\text{circ}} < -500$ km s⁻¹ kpc and 75 km s⁻¹ kpc $< J_R < 200$ km s⁻¹ kpc for $R = 8.2$ kpc, while the OLR is the pointy structure at $J_\phi - J_{\text{circ}} \simeq 500$ km s⁻¹ kpc. Both structures shift with R as expected and in agreement with Fig. 1. The 4:1 resonance appears like a prominent ridge close to $J_\phi - J_{\text{circ}} = 0$.

We also overplot, in the same fashion as figure 4 of Binney (2018), the three regions of resonant trapping in the (J_R, J_ϕ) space (dashed curves), that clearly surround the deformations due to the resonances in our DF computed through Eqs. 3 and 4. We can thus conclude that a slow bar model with $\Omega_b =$

39 km s⁻¹ kpc⁻¹ and the $m = 2$ and $m = 4$ modes of P17 potential is sufficient to create three prominent features in local action space and velocity space.

These qualitative plots, and in particular the one at $R = 8.2$ kpc, can now be compared to data from the Gaia DR2 within 200 pc from the Sun, which we display on Fig. 3, both in the local UV -plane (heliocentric cartesian velocities) and in the plane of epicyclic actions (calculated assuming the P17 background potential and the Sun's peculiar velocities estimates by Schönrich et al. 2010). Interestingly, the three main features generated by the $m = 2$ and $m = 4$ modes of the P17 bar in the UV -plane can be identified in the data if one adopts a peculiar velocity of the Sun of $V_\odot \simeq 10$ km s⁻¹. This is extremely clear for the OLR arch located at $v = 50$ km s⁻¹ in the model and at $V = 40$ km s⁻¹ in the data. Conversely, adopting the peculiar velocity of the Sun of Schönrich et al. (2010), and interpreting the observed arch as the signature of the bar's OLR, then constrains the bar's pattern speed to be $\Omega_b = 39 - 40$ km s⁻¹ kpc⁻¹. However, let us note that it also appears clearly in the data that Hercules is a double-structure, both in velocity space and in action space, with a secondary ridge with velocities V and angular momenta J_ϕ closer to zero, not reproduced by the $m = 2$ and $m = 4$ main resonances in our model.

4. Backward integrations

In our analytical model hereabove, we approximated the true values of the AA using the epicyclic approximation. While this will be cured in further work, we chose to confirm our analytical results here with another technique to obtain the response of the DF to the bar perturbation, the 'backward integrations' used for example by Vauterin & Dejonghe (1997) and Dehnen (2000). This method consists in integrating backwards the orbit of stars all at a certain point \mathbf{x} of configuration space now, but having different velocities on a grid in the (u, v) plane. The method is based on the conservation of the phase-space density. Let us imagine that, at some time $t = t_1$ in the past, the amplitude of the bar was null, and then it started to grow with time until the current configuration at $t = 0$. The value of the DF at $t = t_1$ for the i -th velocity grid point (i.e. an orbit at $(\mathbf{x}, \mathbf{v}_i)$ at $t = 0$) was $f_0(\mathbf{x}_{i,1}, \mathbf{v}_{i,1})$, where $\mathbf{x}_{i,1}$ and $\mathbf{v}_{i,1}$ are the initial position and velocity of the orbit. Then, because of the conservation of phase-space density, its current value at the point \mathbf{x} and the velocity \mathbf{v}_i is

$$f(\mathbf{x}, \mathbf{v}_i) = f_0(\mathbf{x}_{i,1}, \mathbf{v}_{i,1}). \quad (5)$$

This method has to assume an integration time and a law for the growth of the bar. In our case we assume the default values used by Dehnen (2000), i.e., 4 bar rotation for the integration time, a growth of the bar regulated by the polynomial law in equation 4 of Dehnen (2000), and a bar growth time of 2 bar rotations. We assume in this case the full numerical potential by P17, nevertheless with its extension outside of $R = 12$ kpc as in the other Sections. Due to some heating induced by the bar growth, we choose a colder initial DF, with velocity dispersion of 30 km s⁻¹, allowing to more clearly identify the structures, whose locations are independent of the velocity dispersion.

The results of the backward integrations for the same points in configuration space as in Fig. 1 are presented in Fig. 4. From this figure it is clear that the structures with this method are more complex for two main reasons: the presence of moments of the bar at other orders than considered above ($m = 3, m = 5, \dots$), and the ongoing phase-mixing, which adds noise to the backward integrations, especially for long integration times (Fux 2001).

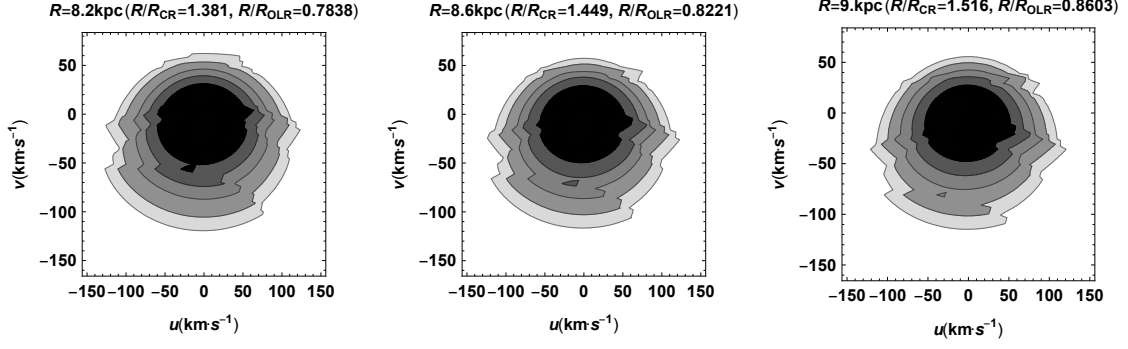


Fig. 1. This figure displays, in local velocity space, the perturbed distribution function obtained through Eqs. 3 and 4 under the influence of the $m = 2$ and $m = 4$ modes of the P17 bar potential, at three particular points of configuration space, $R = R_0 = 8.2$ kpc, $R = 8.6$ kpc, and $R = 9$ kpc, all at the azimuth of the Sun. The axes are u , the Galactocentric radial velocity in the direction of the Galactic center, and v the peculiar tangential velocity with respect to the circular one. The contours enclose (from the inner to the outer 50, 68, 80, 90, and 95 per cent of the star). The position of the point in configuration space compared to the radii of the CR and OLR are shown on each panel's title.

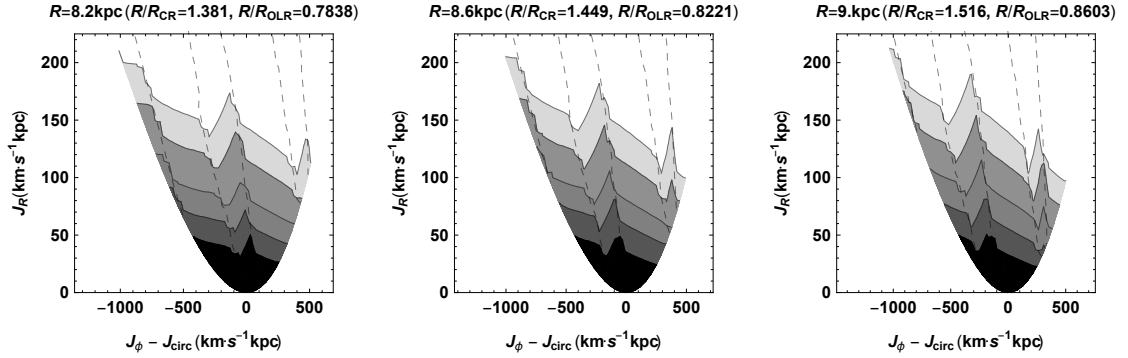


Fig. 2. As in Fig 1 but in action space ($J_\phi - J_{\text{circ}}, J_R$), where J_{circ} is the angular momentum of the circular orbit of the corresponding point in configuration space. The dashed lines enclose the the resonant trapping regions of (from left to right) the CR, the 1:4, and the OLR resonance.

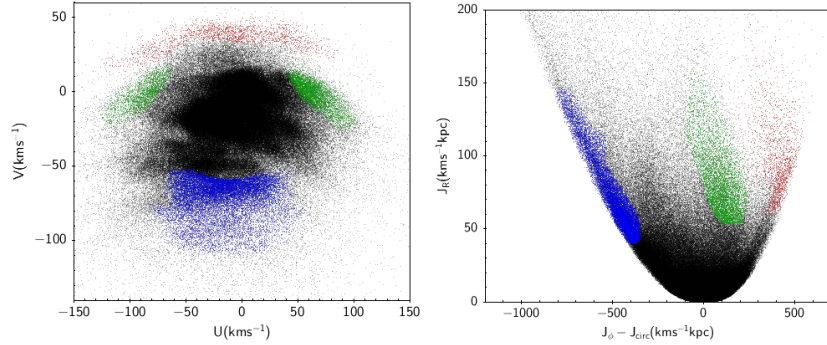


Fig. 3. Left: (U, V) heliocentric velocities of 363796 Gaia DR2 stars with l.o.s. velocities at distances $d < 200$ pc. The distances were computed by Bailer-Jones et al. (2018). Right: the same stars, but in action space as in Fig. 2, assuming the P17 background potential and the peculiar velocity of the Sun by Schönrich et al. (2010). In both panels the same stars are shown with the same colors.

However, it is still possible to distinguish the Hercules moving group, also centred at $(u, v) \simeq (-25, 50)$ km s⁻¹ for $R = 8.2$ kpc and shifting towards lower v as R increases, as in the analytical prediction. One can even identify a secondary structure just above it, reminiscent of the double structure seen in the data. This appears clearer when plotting the result of the backward integration in the space of epicyclic actions, where the CR seems to be accompanied by a secondary ridge at $R = 8.2$ kpc. There is also a very clear secondary ridge accompanying the 4:1 resonance peak in this space at all considered radii, which corresponds to the 3:1 resonance, not included in our analytical model

because we did not extract the $m = 3$ model, to avoid, for the moment, overlaps of resonances. The OLR peak appears only at the very edge of the J_ϕ distribution at $R = 8.2$ kpc, but shifts inwards to lower J_ϕ at larger radii, as expected from the analytical model.

5. Conclusion

In this work have used the analytical method recently developed in Monari et al. (2017a, M17) to study the response of the Galactic disc distribution function to the long bar Galactic potential model developed by Portail et al. (2017, P17). This method is

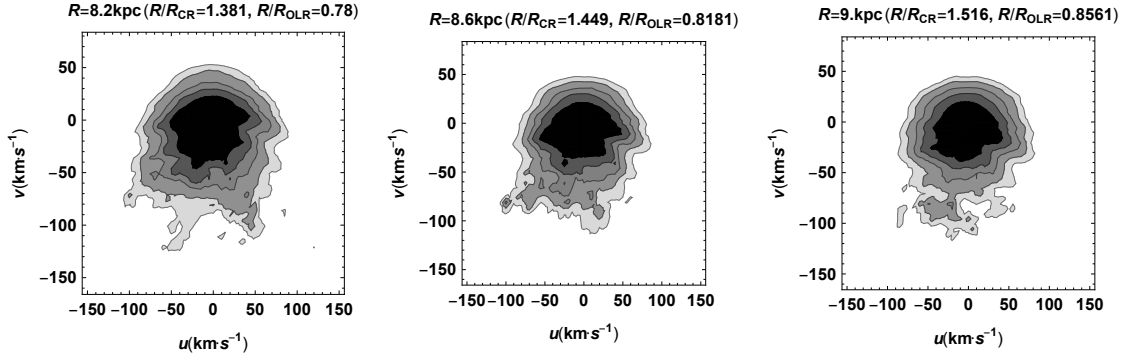


Fig. 4. As in Fig. 1, but with the DF obtained with backward integrations for the full P17 potential. The plot was smoothed with a Gaussian kernel on a scale of 7.5 km s^{-1} .

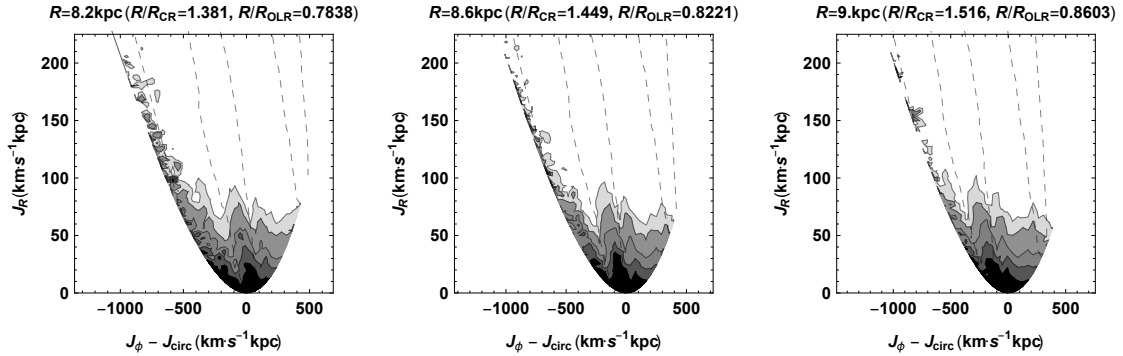


Fig. 5. As in Fig. 2, but for backwards integrations for the full P17 potential.

based on the use of action-angle (AA) coordinates and perturbation theory.

Extracting from this Galactic potential model the $m = 2$ and $m = 4$ components of the bar, we have shown that they deform the disc distribution function in ways that resemble those shown by the second data release of the Gaia satellite around the Sun. In particular, the $m = 2$ modes CR and OLR correspond to features like the Hercules moving group and the high azimuthal velocity arch in the local velocity distribution of stars. The same features can be seen more clearly in action-space both in the model and in the Gaia data. Using the position of the arch in the model and comparing it with the heliocentric velocity of the arch, we can also constrain the peculiar velocity of the Sun to be close to 10 km s^{-1} . Conversely, adopting the peculiar velocity of the Sun of Schönrich et al. (2010), and interpreting the observed arch as the signature of the bar's OLR, then constrains the bar's pattern speed to be $\Omega_b = 39 - 40 \text{ km s}^{-1} \text{ kpc}^{-1}$.

We also perform backward integrations using the whole Galactic bar model (no extraction of modes) that show the same features obtained with the analytical method are also present in velocity and action space, but further complicated by the presence of modes of the bar other than $m = 2$ and $m = 4$, and by on going phase-mixing. Some of these other features can also be related to what is observed in Gaia data release 2.

One caveat of using our method, as implemented in this work, is the use of the epicyclic approximation to estimate AA and orbital frequencies, which is valid only for orbits that deviate little from circularity. In the future we will update these results and extend them to the possibility to describe higher eccentricity orbits using more precise AA and frequencies estimation meth-

ods, like the Stäckel fudge (Sanders & Binney 2016) and the torus machinery (Binney & McMillan 2016; Binney 2018).

The future of the analysis presented in this work, is to perform fits to larger volumes in configuration space, to fully exploit the capabilities of the Gaia data, as well as future spectroscopic surveys such as WEAVE and 4MOST. Better fits to larger volumes of the configuration space will go in parallel with better estimates of the relevant stellar parameters, like, e.g., the distances of the stars from the Sun.

Finally, it would be extremely important to extend perturbation theory methods, like the one used here or the linear theory to study the perturbations of the distribution function far from the resonances (Monari et al. 2016), to the temporal evolution of the perturbations, and to be able to include non-equilibrium phase-mixing effects (Agobert et al. in prep.).

Acknowledgements. This work has made use of data from the European Space Agency (ESA) mission *Gaia* (<https://www.cosmos.esa.int/gaia>), processed by the *Gaia* Data Processing and Analysis Consortium (DPAC, <https://www.cosmos.esa.int/web/gaia/dpac/consortium>). Funding for the DPAC has been provided by national institutions, in particular the institutions participating in the *Gaia* Multilateral Agreement.

References

- Antoja, T., Helmi, A., Romero-Gómez, M., et al. 2018, *Nature*, 561, 360
- Bailer-Jones, C. A. L., Rybizki, J., Fouesneau, M., Mantelet, G., & Andrae, R. 2018, *VizieR Online Data Catalog*, 1347
- Binney, J. 2012, *MNRAS*, 426, 1324
- Binney, J. 2018, *MNRAS*, 474, 2706
- Binney, J. & McMillan, P. 2011, *MNRAS*, 413, 1889
- Binney, J. & McMillan, P. J. 2016, *MNRAS*, 456, 1982
- Binney, J. & Tremaine, S. 2008, *Galactic Dynamics: Second Edition* (Princeton University Press)

- Dehnen, W. 1998, *AJ*, 115, 2384
- Dehnen, W. 1999a, *AJ*, 118, 1190
- Dehnen, W. 1999b, *ApJ*, 524, L35
- Dehnen, W. 2000, *AJ*, 119, 800
- Famaey, B., Jorissen, A., Luri, X., et al. 2005, *A&A*, 430, 165
- Fux, R. 2001, *A&A*, 373, 511
- Gaia Collaboration, Katz, D., Antoja, T., et al. 2018, *A&A*, 616, A11
- Khoperskov, S., Di Matteo, P., Gerhard, O., et al. 2018, *ArXiv e-prints*, arXiv:1811.09205
- Laporte, C. F. P., Minchev, I., Johnston, K. V., & Gómez, F. A. 2018, arXiv:1808.00451 [arXiv:1808.00451]
- Minchev, I., Quillen, A. C., Williams, M., et al. 2009, *MNRAS*, 396, L56
- Monari, G., Famaey, B., Fouvy, J.-B., & Binney, J. 2017a, *MNRAS*, 471, 4314
- Monari, G., Famaey, B., Minchev, I., et al. 2018, *Research Notes of the American Astronomical Society*, 2, 32
- Monari, G., Famaey, B., & Siebert, A. 2016, *MNRAS*, 457, 2569
- Monari, G., Famaey, B., Siebert, A., et al. 2017b, *MNRAS*, 465, 1443
- Monari, G., Kawata, D., Hunt, J. A. S., & Famaey, B. 2017c, *MNRAS*, 466, L113
- Pérez-Villegas, A., Portail, M., Wegg, C., & Gerhard, O. 2017, *ApJ*, 840, L2
- Portail, M., Gerhard, O., Wegg, C., & Ness, M. 2017, *MNRAS*, 465, 1621
- Sanders, J. L. & Binney, J. 2016, *MNRAS*, 457, 2107
- Schönrich, R., Binney, J., & Dehnen, W. 2010, *MNRAS*, 403, 1829
- Sormani, M. C., Binney, J., & Magorrian, J. 2015, *MNRAS*, 454, 1818
- Trick, W. H., Coronado, J., & Rix, H.-W. 2018, *ArXiv e-prints* [arXiv:1805.03653]
- Vauterin, P. & Dejonghe, H. 1997, *MNRAS*, 286, 812
- Wegg, C., Gerhard, O., & Portail, M. 2015, *MNRAS*, 450, 4050
- Weinberg, M. D. 1994, *ApJ*, 420, 597